A Compact Hybrid-Fed Microstrip Antenna for Harmonics-Based Radar and Sensor Systems

Liang Zhu, Nasser Alkhaldi, Haysam M. Kadry, Shaolin Liao, *Senior Member*, *IEEE*, and Pai-Yen Chen, *Senior Member, IEEE*

***Abstract*— In this Letter, we propose and experimentally validate a compact hybrid-fed microstrip antenna for the harmonics-based radar and sensor systems, which receive the fundamental tone and re-transmit the modulated second harmonic. The proposed microstrip antenna is based on a simple single-layered and dual-feed structure, consisting of an inner circular patch operating in the TM_{110} mode (second harmonic; 6 GHz) and an outer split-ring patch operating in the higher-order TM_{210} or TM_{310} mode (fundamental frequency; 3 GHz). By varying the feed position and the geometry of the split-ring patch, specific higher-order mode can be excited at the fundamental frequency. Moreover, analytical expressions were derived for calculating the antenna's resonant frequencies. Our measurement results show that the maximum realized gain is 1.17 dB at 3 GHz and is 3.33 dB at 6 GHz, with good impedance matching ($|S_{11}|$ < -15 dB) and high isolation (< -20 dB).**

***Index Terms*— hybrid-fed antennas, microstrip antennas, harmonic radar, harmonic sensors, higher-order mode excitation.**

I. INTRODUCTION

Wireless sensing, tracking and identification platforms have drawn growing interest in the emerging disciplines of internet-of-things (IoTs), autonomous driving, smart health, and smart cities [1]-[3]. In recent years, passive telemetry based on harmonics detection (e.g., harmonic radar [4]-[10] and harmonic sensors [11]-[16]) has been gaining popularity, thanks to its inherent robustness to clutter, jammer, multipath interference, and crosstalk between Tx/Rx antennas. In these nonlinear backscattering systems, a miniature tag or sensor is based on the passive harmonic transponder, which receives a fundamental tone with frequency f_0, doubling its frequency, and re-transmitting the second harmonic with frequency $2f_0$ to interrogators located in a rich scattering environment, as illustrated in Fig. 1. Since the reader transmits and receives orthogonal frequencies, the influence of unwanted clutters and multi-patch interferences can be considerably suppressed. Very recently, zero-power, miniaturized harmonic sensors have been proposed for IoTs applications, with low power consumption and long read range [11]-[16]. A harmonic sensor typically includes a physically/chemically-sensitive sensor that modulates the strength or peak frequency of the backscattered second harmonic [11]-[16]. Harmonic sensors have been extended to non-invasive detection of critical symbols in medical applications [11]-[14], and remote sensing of temperature and humidity [15],[16].

Although the harmonics-based radar and sensor systems may offer advantages in terms of power and detection range, they usually require two (Rx/Tx) antennas operating at both the fundamental and harmonic frequencies [4]-[16]. This unavoidably increases the total device area and cost. In this Letter, we propose a compact hybrid-fed microstrip patch antenna for the harmonic-based sensing and tracking systems, as schematically shown in Fig. 1. Different from conventional harmonic tags using separate antennas at different frequencies [2], the proposed hybrid-fed structure can significantly reduce the area occupation and can be designed by an approximate analytical model, with versatile means of modal excitation. In addition, such a design does not require additional filters or diplexers. This paper is organized as follows. In Section II, we will first use the cavity model to predict resonant modes and modal field distributions of the proposed microstrip patch antenna, which are important for determining positions of the two feed points. Then, we will conduct the full-wave simulation to verify analytical results. In Section III, we will experimentally study the performance of the proposed antennas by fully characterizing their reflection coefficient, isolation, radiation pattern, and antenna gain. Finally, we will draw a short conclusion in Section IV. Our results show that the proposed hybrid-fed microstrip antennas, although having a compact size and good conformality, can provide satisfactory radiation properties, good impedance matching, and high port isolation.

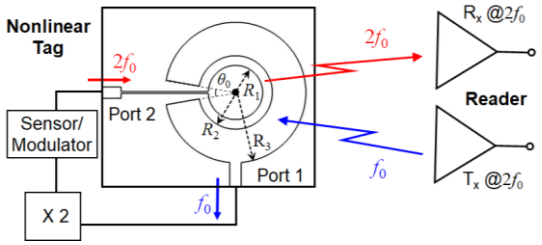

Fig. 1. Schematics of a miniature harmonic transponder based on the proposed hybrid-fed microstrip patch antenna.

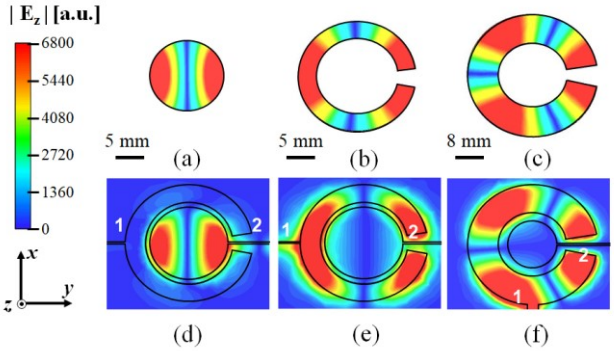

Fig. 2. Snapshots of electric field (E_z) distributions for (a) the TM_{110} mode of a circular-shape cavity, and (b) the TM_{210} mode and (c) the TM_{310} mode of the split annular-ring cavity; here PEC boundaries are assumed at the top and bottom surfaces, while PMC boundaries are assumed on the sidewall. (d)-(f) are similar to (a)-(b), but for simulated results of realistic hybrid-fed microstrip antennas shown in Figs. 3 and 4.

Manuscript received June 11th, 2018.

L. Zhu and P. Y. Chen are with the Department of Electrical and Computer Engineering, University of Illinois, Chicago, IL 60607, USA.

N. Alkhaldi and H. M. Kadry are with the Department of Electrical and Computer Engineering, Wayne State University, Detroit, MI 48202, USA. H. M. Kadry is with the Ford Motor Company, Dearborn, MI 48124, USA.

S. Liao is with the Argonne National Laboratory, Lemont, IL 60439, and the Department of Electrical and Computer Engineering, Illinois Institute of Technology, Chicago, IL 60616.

L. Zhu and N. Alkhaldi contribute equally to this work. Corresponding authors: P. Y. Chen; e-mail: pychen@uic.edu

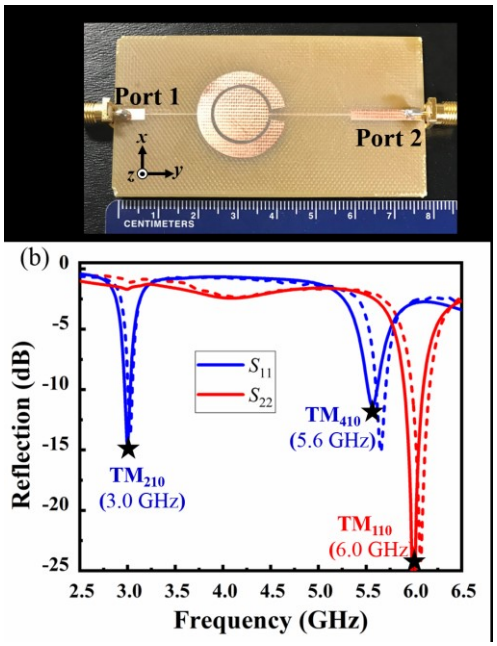

Fig. 3. (a) Photograph of the hybrid-fed microstrip TM_{110}-TM_{210} antenna. (b) The simulated and measured reflection coefficient (S_{11} and S_{22}) of the antenna in (a); here, solid and dash lines respectively represent the simulation and measurement results, and stars represent analytical results obtained from Eqs. (1) and (2).

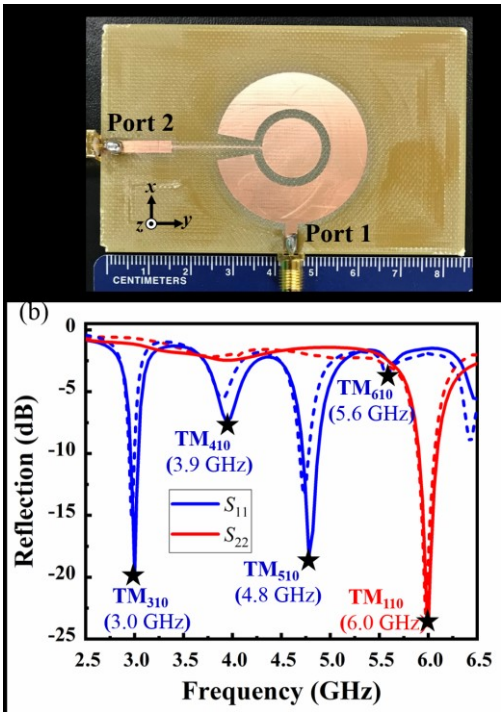

Fig. 4. (a) Photograph of the hybrid-fed microstrip TM_{110}-TM_{310} antenna. (b) The simulated and measured reflection coefficient (S_{11} and S_{22}) of the antenna in (a); here, solid and dash lines respectively represent the simulation and measurement results, and stars represent analytical results obtained from Eqs. (1) and (2).

II. Design and Simulation

Fig. 1 illustrates the geometry of the proposed hybrid-fed microstrip antenna, consisting of a circular patch with radius R_1 and a concentric split-ring patch with inner radius R_2, outer radius R_3, and the cutting angle θ_0. The patch layer is separated from the ground plane by the FR4 substrate with relative permittivity $\varepsilon_r = 4.3$, loss tangent $\delta = 0.015$, and thickness d = 1.5 mm. The operating frequencies of this hybrid-fed antenna can be estimated by using the cavity model [3], where the circular patch and the split-ring patch resonate at the second harmonic ($2f_0$) and the fundamental frequency (f_0), respectively. In each cavity, the perfect electric conductor (PEC) boundary condition is applied at the top and bottom surfaces, and the perfect magnetic conductor (PMC) is assumed on sidewalls. The transcendental equation of the inner cavity, as a function of the radius R_1, can be derived as:

$$J_n'(kR_1) = 0, \quad \text{and} \quad n = 1,\ 2,\ 3\ldots \qquad (1)$$

where $J_n(\cdot)$ and $Y_n(\cdot)$ are the Bessel functions of first and second kinds, $k = \omega\sqrt{\varepsilon_r\varepsilon_0\mu_0}$, ε_0 and μ_0 are free-space permittivity and permeability. The transcendental equation of the outer cavity, as a function of the radii R_2 and R_3, and the cutting angle θ_0, can be derived as:

$$J_n'(kR_2)Y_n'(kR_3) - J_n'(kR_3)Y_n'(kR_2) = 0, \qquad (2a)$$

$$n = m\frac{\pi}{2\pi - \theta_0}, \quad \text{and} \quad m = 1,\ 2,\ 3\ldots \qquad (2b)$$

For the inner circular-patch antenna, the fundamental mode (TM_{110}) is excited at the output frequency $2f_0$, which is controlled by the radius of the circular patch R_1 [Eq. (1)]. Depending on the feed position, the higher-order modes (TM_{210} or TM_{310}) can be excited in the concentric split-ring patch antenna, which governs the input frequency f_0 and is tuned by geometrical parameters (R_2, R_3, θ_0) [Eq. (2)].

We have designed the compact dual-fed patch antenna [Figs. 3 and 4] for a harmonic transponder that receives a fundamental tone at 3 GHz and retransmits a harmonic signal at 6 GHz. The feed position is of importance, as it determines the excitation of specific TM_{mn0} modes. Here, Eqs. (1) and (2) were used to determine the geometrical parameters of the hybrid-fed microstrip antenna. To excite the TM_{210} mode at the fundamental frequency (3 GHz), the parameters of the concentric, split annular-ring patch are: R_2 = 7.6 mm, R_3 = 11 mm, and θ_0 = 20°. Assuming that the operating frequency is the same, the TM_{310} mode is excited when the geometrical parameters are: R_2 = 9 mm, R_3 = 17.2 mm, and θ_0 = 20°. To excite the TM_{110} mode at the second harmonic (6 GHz), the radius of the circular patch R_1 = 7 mm. Here, we note that by optimizing dimensions of the split-ring patch (e.g., R_2 = 3 mm and R_3 = 7 mm), the fundamental mode (TM_{110} mode) can also be excited at 3 GHz. However, the inner/outer radius of the split-ring patch becomes smaller than the radius of the circular path. In this case, the hybrid-fed structure is not feasible. On the other hand, for higher-order resonant modes (e.g, TM_{410} and beyond), the surface current distributions and thus radiation pattern become sophisticated, with a reduced broadside directivity and undesired sidelobes.

We have conducted the full-wave numerical simulation based on the frequency-domain finite-element method to validate the resonant frequencies predicted by the cavity model [17]. Based on the analytical eigenmodal analysis in Figs. 2(a)-(c), we have designed two hybrid-fed patch antennas (TM_{110}-TM_{210} or TM_{110}-TM_{310}) that are fed by microstrip lines connected to two 50 Ω excitation ports (e.g., SMA connector), with suitably designed matching networks. By adjusting the feed point location and the geometry of the split-ring patch, the TM_{210} or TM_{310} mode can be excited at the same frequency (3 GHz). For each mode, the optimum position of the feed point can be obtained by observing the location of maximum field intensities in Figs. 2(b)

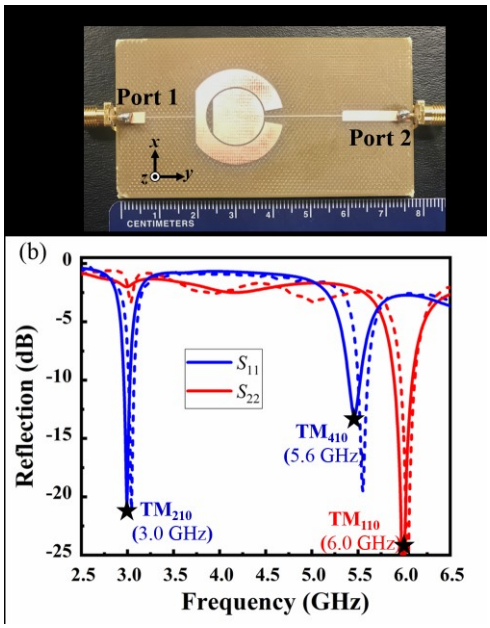

Fig. 5. (a) Photograph of the hybrid-fed TM_{110}-TM_{210} microstrip antenna, whose structure is similar to Fig. 3, but with suitable geometric perturbations for modifying the radiation pattern. (b) The simulated and measured reflection coefficient (S_{11} and S_{22}) of the antenna in (a); here, solid and dash lines respectively represent the simulation and measurement results.

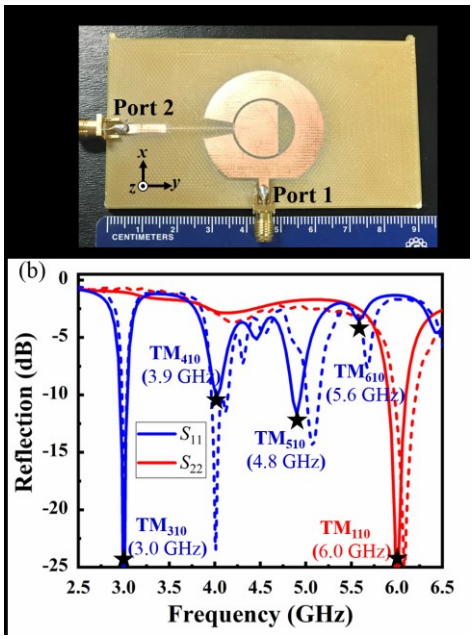

Fig. 7. (a) Photograph of the modified hybrid-fed TM_{110}-TM_{310} microstrip antenna, whose structure is similar to Fig. 4, but with suitable geometric perturbations for modifying the radiation pattern. (b) The simulated and measured reflection coefficient (S_{11} and S_{22}) of the antenna in (a); here, solid and dash lines respectively represent the simulation and measurement. results.

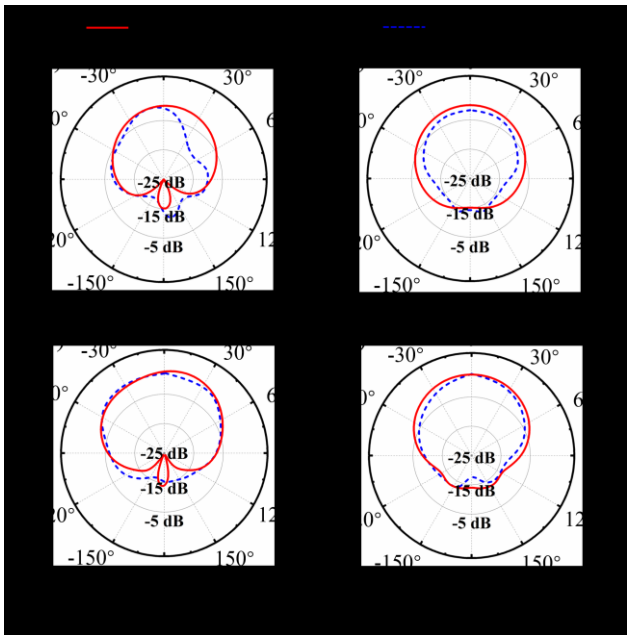

Fig. 6. Simulated and measured radiation patterns for the modified hybrid-fed TM_{110}-TM_{210} antenna in Fig. 5. (a) and (b) are respectively the E-plane and H-plane radiation patterns at 3 GHz. (c) and (d) are respectively the E-plane and H-plane radiation patterns at 6 GHz.

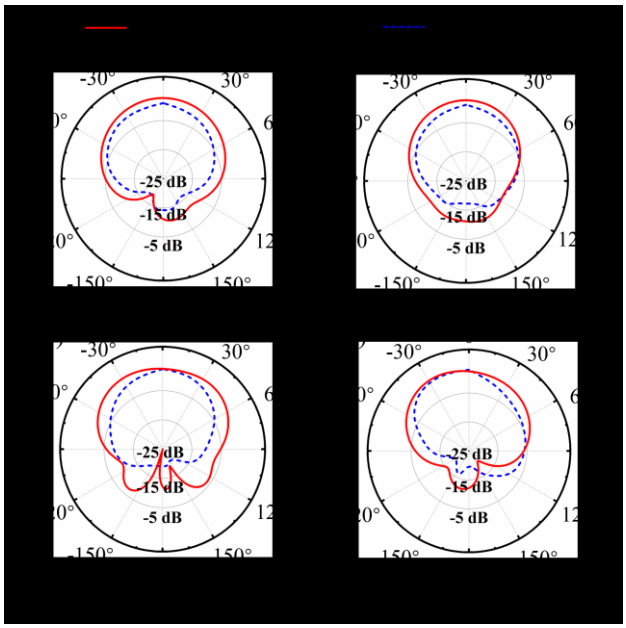

Fig. 8. Simulated and measured radiation pattern for the hybrid-fed antenna in Fig. 7. (a) and (b) are respectively the E-plane and H-plane radiation patterns at 3 GHz. (c) and (d) are respectively the E-plane and H-plane radiation patterns at 6 GHz.

and 2(c). The calculated snapshots of electric field distributions at the resonance frequencies are presented in Figs. 2(d)-(f), in comparison with analytical results in Figs. 2 (a)-(c). Here, we find a good agreement between the full-wave simulation results of the realistic hybrid-fed antennas [Figs. 2(d)-(f)] and those obtained from the analytical eigenmodal analysis [Figs. 2(a)-(c)]. Such results demonstrate the effectiveness of our analytical approach.

III. Measurement Results

Based on the theoretical and numerical results in Section II, we have fabricated and characterized four different types of hybrid-fed antenna for miniature harmonic transponders.

A. Hybrid-fed TM_{110}-TM_{210} microstrip patch antennas

We have fabricated the proposed microstrip antenna using the low-cost printed-circuit board (PCB) technique, with FR4 substrate and copper (Cu) microstrips. Fig. 3(a) shows the fabricated hybrid-fed TM_{110}-TM_{210} patch antenna in Fig. 2(e); here, the received fundamental tone will be guided to port 1 and the frequency-doubled RF signal will be re-radiated through port 2. Fig. 3(b) reports simulated (solid lines) and measured (dashed lines) reflection coefficients, S_{11}versus frequency for the microstrip antenna in Fig. 3(a). It is evident that the measurement and simulation results are in good agreement, with minor variations due to fabrication errors. The analytically predicted resonance frequencies obtained from Eqs. (1)-(2) are also highlighted (stars) in Fig. 3(b). Our measurement results confirm the resonant behaviors of the proposed hybrid-fed patch antenna, with a noticeable dip of S_{11} at 3 GHz (fundamental frequency) and a dip of S_{22} at 6 GHz (second harmonic). Moreover, both simulation and measurement results indicate good impedance matching. The -10 dB bandwidth is 50 MHz at 3 GHz and is 160 MHz at 6 GHz. The measured S_{21} also indicates a < -20 dB isolation between two ports at the fundamental frequency and the second harmonic (not shown here for saving some space). There are also some higher-order modes excited in the inner circular patch (e.g., TM_{410} mode). However, the frequencies of these modes are far from the fundamental and second-harmonic frequencies, and should not affect the port isolation.

Although the proposed hybrid-fed microstrip antenna in Fig. 3 displays the desired operating frequencies, the radiation pattern is somewhat tilted due to the asymmetric current distributions, as the two feed lines could perturb the field distributions. To maximize the broadside radiation and achieve a more symmetric pattern, the patch geometry must be slightly modified. For instance, this task could be accomplished by introducing truncated corners. Fig. 5(a) shows the optimum geometry of the hybrid-fed TM_{110}-TM_{210} microstrip antenna. The geometric perturbation may not only enhance the broadside radiation pattern, but also improve the impedance matching and the realized gain. Fig. 5(b) reports the simulated and measured reflection coefficients versus frequency, showing good isolation and impedance matching at the fundamental and second-harmonic frequencies. Fig. 6 shows the simulated and measured radiation pattern at the operating frequencies. At 3 GHz (TM_{210} mode), this antenna exhibits a maximum realized gain of 1.03 dB, with a half-power beam width (HPBW) of 55° on the E-plane and a HPBW of 93° on H-plane. At 6 GHz (TM_{110} mode), this antenna exhibits a maximum gain of 2.83 dB, with a HPBW of 100° (74°) on the E-plane (H-plane). This hybridized TM_{110}-TM_{210} microstrip antenna may achieve considerable area and cost savings for the size-restricted harmonic transponders.

B. Hybrid-fed TM_{110}-TM_{310} microstrip patch antennas

Figs. 4(a) and 4(b) show the fabricated TM_{110}-TM_{310} hybrid-fed microstrip antenna [Fig. 2(f)] and its measured reflection coefficients, respectively. It is clearly seen that the measurement results (dashed lines) agree quite well with the simulation results (solid lines), and the resonance frequencies can be quantitatively predicted by the analytical model (stars). We note that in this design, other higher-order modes, well predicted by Eqs. (1)-(2) and simulations, are excited in the split-ring patch antenna. However, with properly designed patch geometry, good isolation and impedance matching can still be obtained, as can be seen in Fig. 4(b). There is no resonant mode overlapping with each other, particularly at the two frequencies of interest (3 GHz and 6 GHz). The measured -10 dB bandwidth is 50 MHz at 3 GHz and is 165 MHz at 6 GHz. The measured radiation pattern shows that the main beam is somewhat tilted from the broadside direction (not shown here for saving some space).

We also applied geometric perturbations to the microstrip antenna in Fig. 4, aiming to enhance the directivity at the broadside and improve the symmetricity of radiation pattern. The optimized design is shown in Fig. 7(a). Fig. 7(b) reports the simulated and measured reflection coefficients, showing excellent agreement for all resonant modes. The measured -10 dB bandwidth is 50 MHz at 3 GHz and is 240 MHz at 6 GHz, which are nearly unchanged compared to those of the original design. Fig. 8 shows the simulated and measured radiation patterns for the antenna in Fig. 7. The measured maximum realized gain (TM_{310} mode) is 1.17 dB at 3 GHz, while the value is slightly improved to 3.33 dB at 6 GHz (TM_{110} mode). Compared to the hybrid-fed TM_{110}-TM_{210} microstrip antenna, although the total size of the hybrid-fed TM_{110}-TM_{310} microstrip antenna is somewhat increased, the distance between two feeding ports is reduced. Nonetheless, these two design alternatives have comparable matching and radiation performance, thus offering flexibility in the transponder integration among the antenna and electronic components (e.g., frequency doubler, matching circuit, and sensor). Finally, we should note that due to relatively high dielectric and conduction losses, the measured radiation efficiencies of the above microstrip antennas are 40 %-70 %. The realized gain of the proposed antennas can be further enhanced by using a high-quality PCB substrate with low dissipation factors and by optimizing the shape of microstrip feeds.

IV. Conclusion

We propose new types of conformal and low-profile microstrip patch antennas for miniature harmonic transponders. The proposed hybrid-fed structures have isolated resonances at the fundamental and second-harmonic frequencies, which can be estimated analytically by solving the transcendental equation. Here, we demonstrate that the TM_{110} and TM_{210} (or TM_{310}) modes can be respectively excited at 3 GHz and 6 GHz by tailoring positions of the feed point and the antenna geometry. Our measurement results show a satisfactory antenna gain with symmetrical broadside patterns, as well as good impedance matching and port isolation. The proposed microstrip antennas may benefit various size-restricted harmonic transponders used for harmonic radars, harmonic sensors, medical implants, passive radio-frequency identification (RFID), and internet-of-things (IoT) applications.

References

[1] J. Zhang, G. Y. Tian, A. M. J. Marindra, A. I. Sunny, and A. B. Zhao, "A Review of Passive RFID Tag Antenna-Based Sensors and Systems for Structural Health Monitoring Applications," *Sensors*, vol. 17, no. 265, 2017.

[2] X. L. Jia, Q. Y. Feng, T. H. Fan, and Q. S. Lei, "RFID technology and its applications in Internet of Things (IoT), "*2012 2nd International Conference on Consumer Electronics, Communications and Networks (CECNet)*, pp. 21-23, Yichang, China, 2012.

[3] S. Amendola, R. Lodato, S. Manzari, C. Occhiuzzi, and G. Marrocco, "RFID Technology for IoT-Based Personal Healthcare in Smart Spaces," *IEEE Internet Of Things Journal*, vol. 1, no. 2, pp. 144-152, 2014.

[4] J. R. Riley, A. D. Smith, D. R. Reynolds, A. S. Edwards, J. L. Osborne, I. H. Williams, et al, "Tracking bees with harmonic radar," *Nature*, vol. 379, pp. 29-30, 1996.

[5] L. Chioukh, H. Boutayeb, D. Deslandes, and K. Wu,, "Noise and sensitivity of harmonic radar architecture for remote sensing and detection of vital signs," *IEEE Trans. Microw. Theory. Techn*, vol. 62, no. 9, 2014.

[6] B. Kubina, J. Romeu, C. Mandel, M. Schüßler, and R. Jakoby, "Quasi-chipless wireless temperature sensor based on harmonic radar," *Electron. Lett*, vol. 50, no. 2, pp. 86-88, 2014.

[7] K. Rasilainen, J. Ilvonen, A. Lehtovuori, J. M. Hannula, and V. Viikari, "On design and evaluation of harmonic transponders," *IEEE Trans. Antennas Propag*, vol. 63, no. 1, pp. 15-23, 2015.

[8] K. Rasilainen, J. Ilvonen, J. M. Hannula, and V. Viikari, "Designing Harmonic Transponders Using Lumped-Component Matching Circuits, " *IEEE Antennas and Wireless Propag. Lett.*, vol. 16, pp. 246-249, 2017.

[9] Z. M. Tsai, P. H. Jau, N. C. Kuo, J. C. Kao, K. Y. Lin, F. R. Chang, et al, "A High-Range-Accuracy and High-Sensitivity Harmonic Radar Using

Pulse Pseudorandom Code for Bee Searching," *IEEE Trans. Microw. Theory. Techn*, vol. 61, no. 1, pp. 666-675, 2012.

[10] D. Psychoudakis, W. Moulder, C. C. Chen, H. P. Zhu, and J. L. Volakis, "A portable low-power harmonic radar system and conformal tag for insect tracking," *IEEE Antennas and Wireless Propag. Lett.*, vol. 7, pp. 444-447, 2008.

[11] H. Huang, L. Tao, F. Liu, L. Ji, Y. Hu, M. C. Cheng, P. Y. Chen, and D. Akinwande, "Chemical-sensitive graphene modulator with a memory effect for internet-of-things applications," *Microsystems and Nanoengineering*, vol. 2, p. 16018, 2016.

[12] H. Huang, P. Y. Chen, C. H. Hung, R. Gharpurey, and D. Akinwande, "A zero power harmonic transponder sensor for ubiquitous wireless μL liquid-volume monitoring," *Sci. Rep*., vol. 6, p. 18795, 2016.

[13] M. Hajizadegan, M. Sakhdari, L. Zhu, Q. Cui, H. Huang, M. C. Cheng, J. Hung, and P. Y. Chen, "Graphene Sensing Modulator: Toward Low-Noise, Self-Powered Wireless Microsensors," *IEEE Sens. J*., vol. 17, no. 22, pp. 7239 - 7247, 2017.

[14] H. Y. Huang, M. Sakhdari, M. Hajizadegan, A. Shahini, D. Akinwande, and P. Y. Chen, "Toward transparent and self-activated graphene harmonic transponder sensors," *Appl. Phys. Lett.*, vol. 108, no. 17, p. 173503, 2016.

[15] F. Alimenti, and L. Roselli, "Theory of zero-power RFID sensors based on harmonic generation and orthogonally polarized antennas," *Progress in Electromagnetics Research*, vol. 134, pp. 337-357, 2013.

[16] A. Lazaro, R. Villarino, and D. Girbau, "A Passive Harmonic Tag for Humidity Sensing," *International Journal of Antennas and Propagation*, vol. 2014, 670345, 2014.

[17] CST Microwave Studio: http://www.cst.com